Nanoscale Res Lett (2009) 4:558–564
DOI 10.1007/s11671-009-9280-3

NANO EXPRESS

Synthesis, Optical Properties, and Photocatalytic Activity of One-Dimensional CdS@ZnS Core-Shell Nanocomposites

Le Wang · Hongwei Wei · Yingju Fan · Xinzheng Liu · Jinhua Zhan

Received: 30 December 2008 / Accepted: 16 February 2009 / Published online: 5 March 2009

Abstract One-dimensional (1D) CdS@ZnS core-shell nanocomposites were successfully synthesized via a two-step solvothermal method. Preformed CdS nanowires with a diameter of ca. 45 nm and a length up to several tens of micrometers were coated with a layer of ZnS shell by the reaction of zinc acetate and thiourea at 180 °C for 10 h. It was found that uniform ZnS shell was composed of ZnS nanoparticles with a diameter of ca. 4 nm, which anchored on the nanowires without any surface pretreatment. The 1D CdS@ZnS core-shell nanocomposites were confirmed by XRD, SEM, TEM, HR-TEM, ED, and EDS techniques. The optical properties and photocatalytic activities of the 1D CdS@ZnS core-shell nanocomposites towards methylene blue (MB) and 4-chlorophenol (4CP) under visible light ($\lambda > 420$ nm) were separately investigated. The results show that the ZnS shell can effectively passivate the surface electronic states of the CdS cores, which accounts for the enhanced photocatalytic activities of the 1D CdS@ZnS core-shell nanocomposites compared to that of the uncoated CdS nanowires.

Keywords Nanocomposites · Nanowires · Semiconductor · Photocatalysis · Cadmium sulfide

Introduction

One-dimensional (1D) nanocomposites consisting of two important functional materials have attracted significant attention with respect to their fascinating properties and potential applications in the field of nanodevice fabrication [1–3]. Superior or new properties and diverse functions have been realized by assembling different types of constituents into nanocomposites with controlled structure and interface interactions. Recently, considerable research efforts have been directed on the shape and compositional control of 1D semiconductor-included nanocomposites, such as nanowires with superlattice structures [4, 5], core-shell coaxial nanowires [6–13], biaxial or sandwich-like triaxial nanowires [14–18], and anisotropic (e.g., dimer-type and hierarchical composite materials) heterostructures [19–23]. In particular, core-shell nanostructures are reported most often because various mechanisms can be involved in shell growth that do not necessarily relate to epitaxy between the inorganic components, and consequently enhanced or modified properties are resulted from the particular dimensionality. For example, Lieber et al. [24] have reported on the synthesis of Ge/Si core-shell nanowires (NW) and high-performance as field-effect transistors due to the reduced interface scattering. Xu et al. [25] demonstrated that Ni nanowires encapsulated within fullerene cables exhibited enhanced and anisotropic ferromagnetic behavior along the nanowire axes.

The development of new heterostructures is still a challenging subject, for the critical step of this work remains how to modulate the properties by tailoring the nucleation of one phase on the surface of the other. Wurtzite CdS, a direct band gap semiconductor with a gap energy of 2.42 eV at 300 K, is one of the first discovered semiconductors which has promising applications in photochemical catalysis, gas sensor, detectors for laser and infrared, solar cell, nonlinear optical materials, various luminescence devices, and optoelectronic devices [26–28]. On the account of this, various 1D CdS nanostructural materials have been generated through various routes

L. Wang · H. Wei · Y. Fan · X. Liu · J. Zhan (✉)
Department of Chemistry and Chemical Engineering, Shandong University, Jinan 250100, People's Republic of China
e-mail: jhzhan@sdu.edu.cn

[29–32]. ZnS has a wider band gap ($E_g = 3.7$ eV) than CdS. The surface modification of a wide band gap semiconducting shell around a narrow band gap core can alter the charge, functionality, and reactivity of the materials and consequently enhance the functional properties due to localization of the electron-hole pairs [33–35]. Up to now, CdS@ZnS core-shell nanostructures with stronger luminescence and electrical properties have been successfully prepared by metal-organic CVD (MOCVD) process or wet–chemical approach [10, 36–38].

In this paper, we try to use preformed CdS nanowires as 1D nanoscale substrates for the growth of ZnS shell by a two-step solution method. No surface pretreatments were needed to introduce new surface functional groups, or additional covalent and/or noncovalent interconnectivity for the growth of ZnS onto CdS nanowires in our experiments. The optical properties and photocatalytic activities of the 1D CdS@ZnS core-shell nanocomposites under visible light ($\lambda > 420$ nm) were investigated. The results show that the ZnS shell can effectively passivate the surface electronic states of the CdS cores, which helps to enhance the photocatalytic activities of the 1D CdS@ZnS core-shell nanocomposites.

Experimental Section

The Preparation of 1D CdS@ZnS Core-Shell Nanocomposites was Achieved via a Two-Step Solvothermal Process. All Reagents were Analytical Grade and were Used Without Further Purification

Preparation of CdS Nanowire

In a typical process, $Cd(S_2CNEt_2)_2$ (1.124 g, 0.1 mmol) prepared by precipitation from a stoichiometric mixture of NaS_2CNEt_2 and $CdCl_2$ in water, was added to a Teflon-lined stainless steel autoclave with a capacity of 55 mL. Then the autoclave was filled with 40 mL ethylenediamine up to about 70% of the total volume. The autoclave was maintained at 180 °C for 24 h and then allowed to cool to room temperature. A yellowish precipitate was collected and washed with absolute ethanol and distilled water to remove residue of organic solvents. The final products were dried in vacuum at 70 °C for 6 h.

Preparation of 1D CdS@ZnS Core-Shell Nanocomposites

As a general procedure, CdS nanowires (0.03 g, 0.2 mmol) were well-dispersed in 45 mL absolute ethanol under sonication, then $Zn(CH_3COO)_2 \cdot 2H_2O$ (0.022 g, 0.1 mmol) and $(NH_2)_2CS$ (0.015 g, 0.2 mmol) were added in sequence. The resulting mixture was loaded into a 55 mL-Telfon-lined autoclave and maintained at 180 °C for 12 h. After the reaction was completed, the autoclave was cooled to room temperature naturally, and the resulting solid products were collected, washed with absolute ethanol and distilled water for twice, and then dried in vacuum at 70 °C for 6 h.

Characterization

The crystal structure of the product was determined from the X-ray diffractometer (Bruker D8) with a graphite monochromator and Cu $K\alpha$ radiation ($\lambda = 1.5418$ Å) in the range of 15–80° at room temperature while the tube voltage and electric current were held at 40 kV and 20 mA. The morphology and microstructure of the products were determined by FESEM (Hitachi S-4800), TEM (JEM-100CXII) with an accelerating voltage of 80 kV, and high-resolution TEM (HR-TEM, JEOL-2100) with an accelerating voltage of 200 kV equipped with an energy-dispersive X-ray spectrometer (EDS). The UV-vis spectra and room photoluminescence (PL) were performed on a TU-1901 UV-vis spectrophotometer and WGY-10 spectrofluorimeter.

Photocatalytic Decomposition of MB and 4CP

To evaluate the photocatalytic activity of the synthesized 1D CdS@ZnS core-shell nanocomposites, the degradation of MB and 4CP were carried out in a jacketed quartz reactor filled with 50 mL of the test solution in the presence of the catalyst (50 mg) by using a 300-W Xe lamp with a cutoff filter ($\lambda > 420$ nm) as light source. Prior to illumination, the suspension was stirred for 20 min in the dark to favor the pollutant's adsorption onto the catalyst surface, followed by determination of the concentration of the pollutants as the initial concentration C_0. The remaining concentration of pollutants in the suspension at given intervals of irradiation was measured on a TU-1901 UV-vis spectrophotometer.

Results and Discussion

Characterizations of the Final Products

The CdS nanowires and 1D CdS@ZnS hybrid nanocomposites were analyzed using XRD, SEM, TEM, and HRTEM to evaluate the structural characteristics. Figure 1a shows the powder XRD pattern from unmodified CdS nanowires, which can be indexed to the wurtzite structure (JCPDS No. 41-1049). Compared with the standard card, the diffraction peaks of (100) and (110) are relatively strong, while the peak of (002) is weak, which can attributed to the fact that CdS nanowires mainly lie on the experimental cell during the XRD measurement process and have

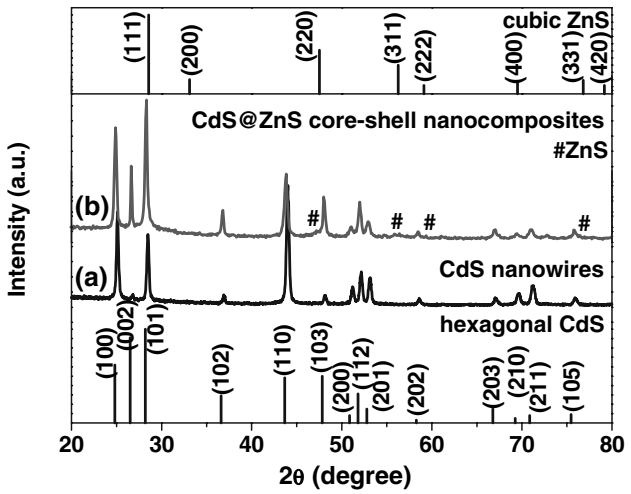

Fig. 1 XRD patterns (**a**) of CdS nanowires and (**b**) of 1D CdS@ZnS core-shell nanocomposites. The stick spectra represent the standard reflections for bulk cubic ZnS and hexagonal CdS, respectively

a preferential orientation along [001] [39]. After ZnS shells are coated onto the CdS nanowires, additional diffraction peaks marked with "#" appear in the XRD pattern (Fig. 1b) corresponding to the powder diffraction pattern for zinc blende ZnS (JCPDS No. 05-0566).

As seen in a SEM image (Fig. 2a), numerous CdS nanowires with a diameter of ca. 45 nm and a length up to several decades of μm are uniformly distributed on the carbon conductive tape. In Fig. 2b, a representative SEM image of 1D CdS@ZnS hybrid nanocomposites, demonstrated that the diameter of the core-shell nanowires had increased to be about ~60 nm while the thickness of the shell layer was calculated to be 5 ~ 10 nm. After the shell growth, the surface of the nanowires became rough (inset of Fig. 2b). The XRD and SEM results indicate that the as-grown product is a composite material of CdS and ZnS with a 1D morphology. Detailed microstructures of the product were further investigated using TEM, HRTEM, ED, and EDS techniques.

TEM image of neat CdS nanowires with smooth surface are shown in Fig. 3a, and a high-magnified TEM image of the marked region in Fig. 3a shows that the CdS nanowires have a highly crystalline nature with a lattice plane separation of 0.335 nm corresponding to the (002) lattice spacing distance of hexagonal CdS (Fig. 3b), which suggests that the CdS nanowires preferentially grow along the [001] direction. The SAED pattern (inset of Fig. 3a) of a single nanowire is also consistent with the single crystalline nature of CdS indexed as the [010] zone axis. In Fig. 3c, the CdS nanowire is coated with a thin layer of ZnS shell, resulting in increased diameter and a relatively rough surface. Figure 3d is an enlargement of the marked region in Fig. 3c, from which we can see the shell is made up of ZnS nanoparticles of ~4 nm diameter growing along

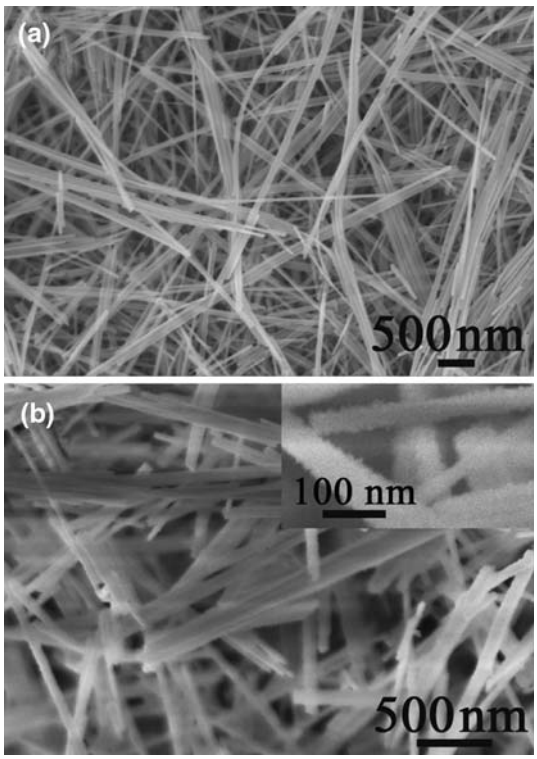

Fig. 2 SEM images (**a**) of CdS nanowires and (**b**) of 1D CdS@ZnS core-shell nanocomposites

the surface of the CdS nanowires. ZnS nanoparticles mainly show two sets of lattice fringe spacings of 0.27 nm and 0.19 nm that correspond to the (200) and (220) planes of the zinc blende ZnS, respectively. The corresponding select area electron diffraction (SAED) pattern of the CdS@ZnS nanocomposite is mainly composed of two sets of diffraction patterns. The dashed parallelogram is indexed as that of hexagonal CdS along the $[2\,\bar{4}\,1]$ zone axis and diffraction rings as that of the ZnS layer with polycrystalline nature (Fig. 3f). The measured lattice spacing based on the rings in the diffraction pattern can separately be indexed as corresponding *hkl* from the PDF database of zinc blende ZnS.

The existence of ZnS layer on the surface of CdS nanowires was further confirmed by EDS data (Fig. 3e). EDS analysis conducted on the central region of a CdS@ZnS core-shell nanowire indicates that the nanowire is mainly composed of Cd, Zn and S with Cd/Zn/S ratio of 0.62:0.36:1 (a stoichiometry close to $Cd_xZn_{1-x}S$). The Cu peaks were detected from the grid for TEM observation.

Optical Properties and Photocatalytic Activity of 1D CdS@ZnS Core-Shell Nanocomposites

The optical properties of 1D CdS@ZnS core-shell nanocomposites were measured using UV-vis absorption and PL spectroscopy. The UV-vis absorption spectra of the

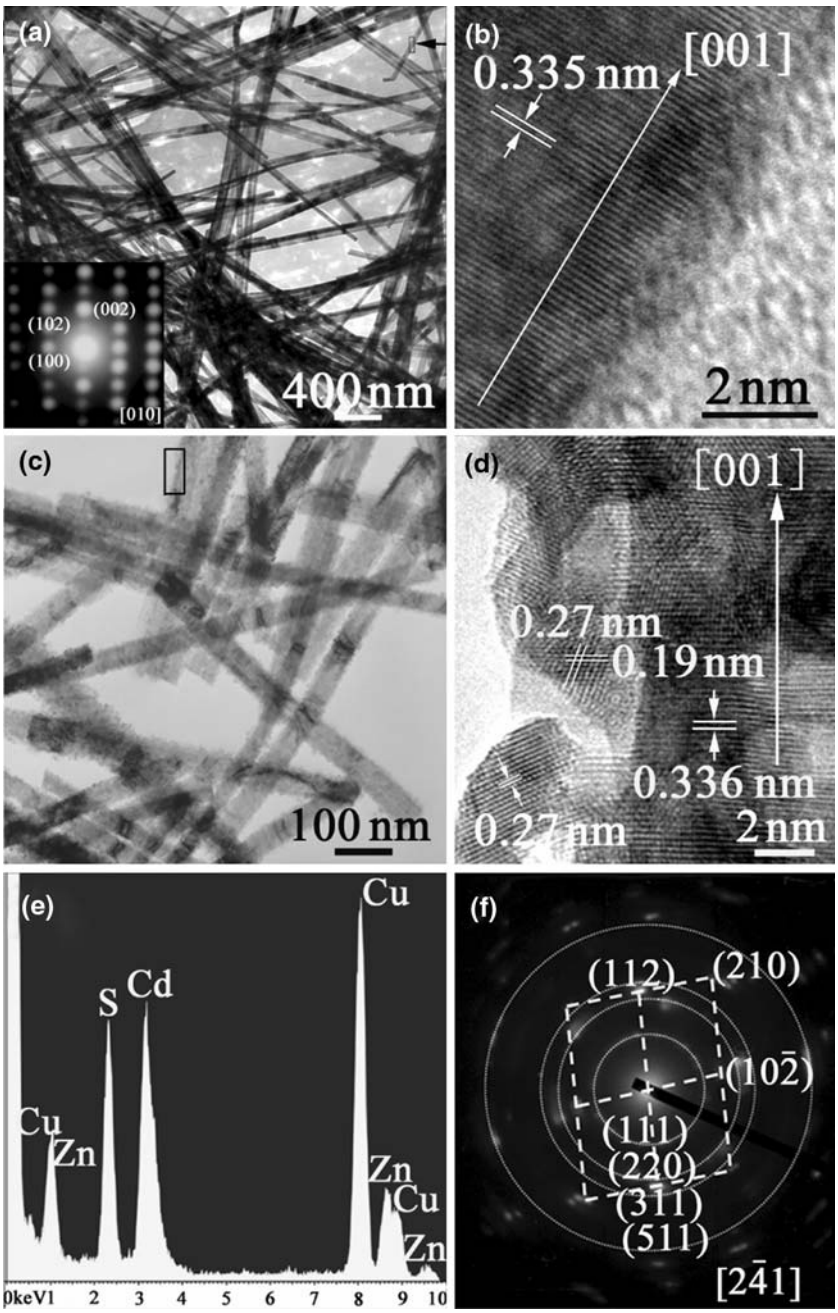

Fig. 3 **a** TEM images of CdS nanowires; inset shows the single crystalline SAED pattern. **b** HRTEM image of the rectangular region of a single CdS nanowire in **a**. (**c**–**f**) TEM images, HRTEM image of the rectangular region in **c** EDS spectrum and SAED pattern with planes of CdS or ZnS indicated separately for the 1D CdS@ZnS core-shell nanocomposites

CdS nanowires and CdS@ZnS core-shell nanocomposites are shown in Fig. 4a. The absorption spectra of the nanocomposites is dominated by the CdS core with a slight blue-shift owning to the influence of the ZnS shells [40]. PL spectra recorded with a 300 nm excitation wavelength are shown in Fig. 4b. The PL spectrum of the uncoated CdS nanowires shows an obvious absorption shoulder around 523 nm, and the PL emission of the nanocomposites exhibits a more intense emission positioned at ~520 nm. The nearly unchanged emission peak position mainly suggests the PL behavior of the CdS nanowires, while it is slightly asymmetric indicating the presence of another emission band toward the higher wavelength region [37]. The enhancement in the emission is due to the fact that high band gap ZnS shell material suppresses the tunneling of the charge carriers from the CdS nanowires to the surface atoms of the shell, resulting in more photogenerated electrons and holes confined inside the CdS cores. Consequently, passivated nonradiative recombination sites that exist on the core surfaces lead to high PL efficiency [41, 42].

The photocatalytic activities of as-obtained 1D CdS@ZnS nanocomposites were evaluated by degradation of MB and 4CP molecules under visible light irradiation

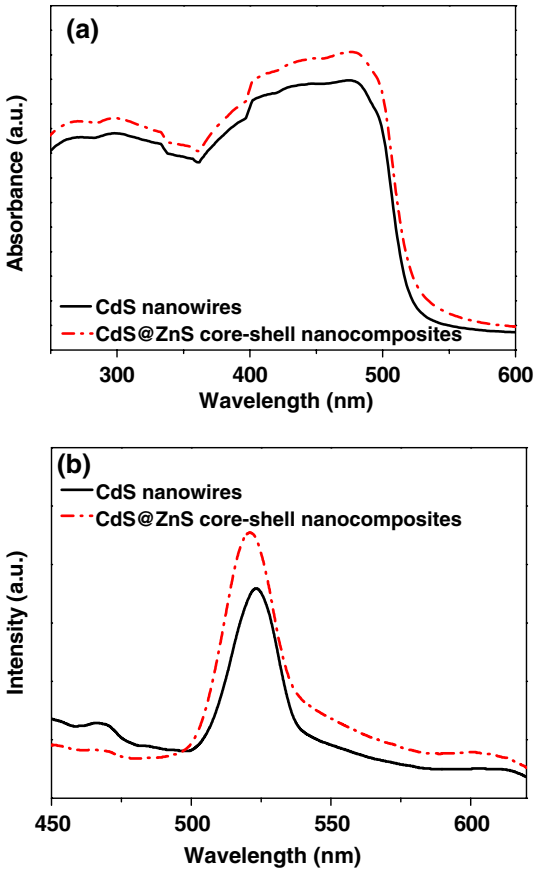

Fig. 4 (**a**) UV-vis spectra and (**b**) room temperature PL spectra (excitation wavelength: 400 nm) of CdS nanowires and 1D CdS@ZnS core-shell nanocomposites

($\lambda > 420$ nm). MB was used as a test contaminant since it has been extensively used as an indicator for the photocatalytic activities [43, 44]. And its degradation can be easily monitored by optical absorption spectroscopy. Figure 5a shows the photocatalytic activities of the nanocomposites evaluated by degradation of MB. The absorption spectral changes when the MB aqueous solution was degraded with the 1D CdS@ZnS core-shell nanocomposites for 6 h. The intensity of the main absorption peaks decreased or even disappeared due to the degradation of MB, and blue-shifted due to the formation of the demethylated dyes [45]. As a comparison, the photodegradation with CdS nanowires (curve 2 in Fig. 5b), with commercial Anatase TiO_2 (curve 3), photolysis in the absence of photocatalyst (curve 4), and with 1D CdS@ZnS nanocomposites in dark (curve 5) were also measured. The *y*-axis of degradation is referred as C/C_0 in which C was the concentration of MB at each irradiated time interval determined at a wavelength of 664 nm while C_0 was the starting concentration when adsorption–desorption equilibrium was achieved. From the chart, it can be seen that MB hardly decomposed under the presence of 1D nanocomposites without irradiation (curve 5). However, the absorption of MB disappeared (99.9% decomposed) after 6 h of visible light irradiation for the 1D nanocomposites (curve 1), showing much greater activity than that of CdS nanowires (63% decomposed, curve 2). In the meantime, up to 67.9% (curve 3) and 52.0% (curve 4) of MB was degraded in the presence of Anatase TiO_2 or only through photolysis, respectively.

Phenolic compounds are widely used in various fields, most of which are highly toxic and can remain in the environment for a longer time due to their stability and bioaccumulation [46]. Photocatalytic treatment is a preferable approach to treat such wastewaters [47, 48]. Absorption spectral changes of 4CP aqueous solution degraded by 1D CdS@ZnS core-shell nanocomposites with different irradiation time are shown in Fig. 6a. Figure 6b shows the change of concentration of 4CP over time under different conditions (C was the concentration of 4CP determined at a wavelength of 225 nm). Control experiments indicated that the photocatalytic reaction hardly proceeded in the absence of visible light (curve 5). After

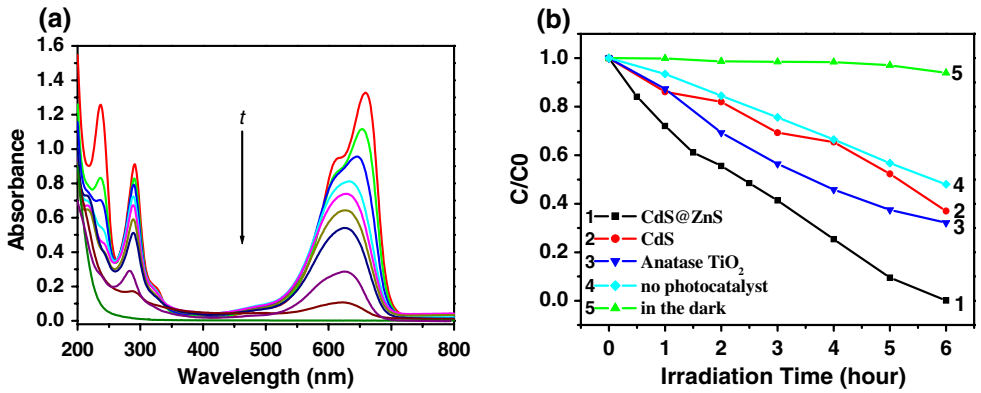

Fig. 5 Absorption spectral changes of MB aqueous solution (15 mg/L) degraded by 1D CdS@ZnS core-shell nanocomposites with irradiation time *t*: 0, 0.5, 1, 1.5, 2, 2.5, 3, 4, 5, and 6 h (**a**). Visible-light Photodegradation of MB under different conditions. Curves: (1) with CdS@ZnS core-shell nanocomposites, (2) with CdS nanowires, (3) with commercial Anatase TiO_2, (4) without any photocatalyst, and (5) with CdS@ZnS core-shell nanocomposites in dark (**b**)

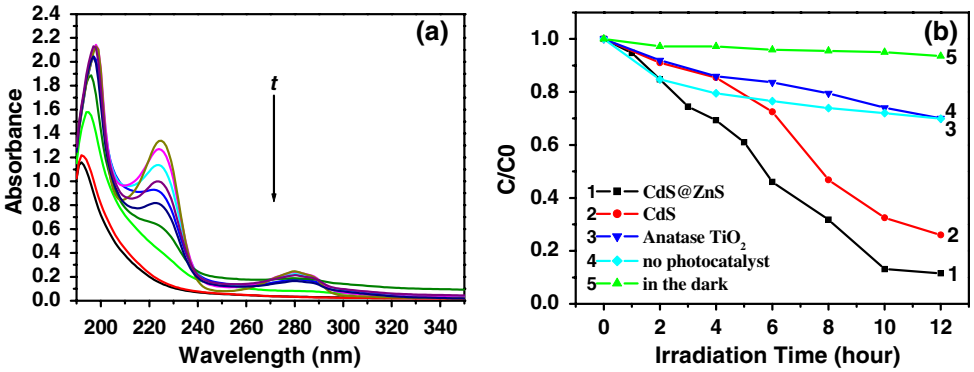

Fig. 6 Absorption spectral changes of 4CP aqueous solution (20 mg/L) degraded by 1D CdS@ZnS core-shell nanocomposites with irradiation time *t*: 0, 1, 2, 3, 4, 5, 6, 8, 10, and 12 h (**a**). Visible-light Photodegradation of 4CP under different conditions. Curves: (1) with CdS@ZnS core-shell nanocomposites, (2) with CdS nanowires, (3) with commercial Anatase TiO_2, (4) without any photocatalyst, and (5) with CdS@ZnS core-shell nanocomposites in dark (**b**)

12 h irradiation, up to 74.0% (curve 2), 30.0% (curve 3), and 30.1% (curve 4) of 4CP was degraded in the presence of CdS nanowires, anatase TiO_2, or only through photolysis, respectively. For the 1D CdS@ZnS nanocomposites, ca. 88.5% of 4CP was degraded under the same conditions (curve 1), showing significantly improved photocatalytic activity than others. The enhanced photocatalytic activity may be due to the surface charge modification and surface electronic states passivation of CdS cores by the ZnS shells.

Conclusion

In summary, 1D CdS@ZnS core-shell nanocomposites were successfully synthesized via a two-step mild solution method. It has been demonstrated that preformed CdS nanowires with a diameter of ca. 45 nm and a length up to several tens of micrometers were coated with a uniform layer of ZnS shell. This shell was composed of ZnS nanoparticles with a diameter of ca. 4 nm, anchoring on the surface of CdS nanowires without any surface pretreatment or functionalization. The optical properties and photocatalytic activities of the 1D nanocomposites under visible light were separately investigated. Compared to the neat CdS nanowires, the as-obtained 1D CdS@ZnS core-shell nanocomposites showed significantly enhanced photocatalytic activities owning to the effective passivation of the surface electronic states by the ZnS shells.

References

1. Y. Wu, J. Xiang, C. Yang, W. Lu, C.M. Lieber, Nature **430**, 61 (2004). doi:10.1038/nature02674
2. U.K. Gautam, X. Fang, Y. Bando, J. Zhan, D. Golberg, ACS Nano **2**, 1015 (2008). doi:10.1021/nn800013b
3. A. Jensen, J.R. Hauptmann, J. Nygrd, J. Sadowski, P.E. Lindelof, Nano Lett. **4**, 349 (2004). doi:10.1021/nl0350027
4. M.S. Gudiksen, L.J. Lauhon, J. Wang, D.C. Smith, C.M. Lieber, Nature **415**, 617 (2002). doi:10.1038/415617a
5. R. Solanki, J. Huo, J.L. Freeouf, B. Miner, Appl. Phys. Lett. **81**, 3864 (2002). doi:10.1063/1.1521570
6. Y. Zhang, K. Suenaga, C. Colliex, S. Iijima, Science **281**, 973 (1998). doi:10.1126/science.281.5379.973
7. S. Han, C. Li, Z.Q. Liu, B. Lei, D.H. Zhang, W. Jin, X.L. Liu, T. Tang, C.W. Zhou, Nano Lett. **4**, 1241 (2004). doi:10.1021/nl049467o
8. X.Y. Kong, Y. Ding, Z.L. Wang, J. Phys. Chem. B **108**, 570 (2004). doi:10.1021/jp036993f
9. J.Q. Hu, Q. Li, X.M. Meng, C.S. Lee, S.T. Lee, Chem. Mater. **15**, 305 (2003). doi:10.1021/cm020649y
10. Y.J. Hsu, S.Y. Lu, Chem. Commun. (Camb.) **18**, 2102 (2004). doi:10.1039/b403932g
11. T. Mokari, U. Banin, Chem. Mater. **15**, 3955 (2003). doi:10.1021/cm034173+
12. L. Manna, E.C. Scher, L.S. Li, A.P. Alivisatos, J. Am. Chem. Soc. **124**, 7136 (2002). doi:10.1021/ja025946i
13. S. Kar, S. Santra, H. Heinrich, J. Phys. Chem. C **112**, 4036 (2008). doi:10.1021/jp800277x
14. Z.L. Wang, Z.R. Dai, R.P. Gao, Z.G. Bai, J.L. Gole, Appl. Phys. Lett. **77**, 3349 (2000). doi:10.1063/1.1327281
15. J. Hu, Y. Bando, Z. Liu, T. Sekiguchi, D. Golberg, J. Zhan, J. Am. Chem. Soc. **125**, 11306 (2003). doi:10.1021/ja0302351
16. R.R. He, M. Law, R. Fan, F. Kim, P.D. Yang, Nano Lett. **2**, 1109 (2002). doi:10.1021/nl0257216
17. J.H. Zhan, Y. Bando, J.Q. Hu, T. Sekiguchi, D. Golberg, Adv. Mater. **17**, 225 (2005). doi:10.1002/adma.200400585
18. B.K. Teo, C.P. Li, X.H. Sun, N.B. Wong, S.T. Lee, Inorg. Chem. **42**, 6723 (2003). doi:10.1021/ic034397u
19. Y. Zheng, L. Zheng, Y. Zhan, X. Lin, Q. Zheng, K. Wei, Inorg. Chem. **46**, 6980 (2007). doi:10.1021/ic700688f
20. J.Y. Lao, J.G. Wen, Z.F. Ren, Nano Lett. **2**, 1287 (2002). doi:10.1021/nl025753t
21. Y. Jung, D.K. Ko, R. Agarwal, Nano Lett. **7**, 264 (2007). doi:10.1021/nl0621847
22. S. Bae, H. Seo, H. Choi, J. Park, J. Park, J. Phys. Chem. B **108**, 12318 (2004). doi:10.1021/jp048918q
23. Y.Q. Li, J.X. Tang, H. Wang, J.A. Zapien, Y.Y. Shan, S.T. Lee, Appl. Phys. Lett. **90**, 093127 (2007). doi:10.1063/1.2710743
24. L.J. Lauhon, M.S. Gudiksen, D.L. Wang, C.M. Lieber, Nature **420**, 57 (2002). doi:10.1038/nature01141

25. F. Tao, Y. Liang, G. Yin, D. Xu, Z. Jiang, H. Li, M. Han, Y. Song, Z. Xie, Z. Xue, J. Zhu, Z. Xu, L. Zheng, X. Wei, Y. Ni, Adv. Funct. Mater. **17**, 1124 (2007). doi:10.1002/adfm.200600177
26. R. Agarwal, C. Barrelet, C.M. Lieber, Nano Lett. **5**, 917 (2005). doi:10.1021/nl050440u
27. R. Ma, L. Dai, G. Qin, Nano Lett. **7**, 868 (2007). doi:10.1021/nl062329+
28. J.S. Jie, W.J. Zhang, Y. Jiang, X.M. Meng, Y.Q. Li, S.T. Lee, Nano Lett. **6**, 1887 (2006). doi:10.1021/nl060867g
29. M. Chen, Y. Xie, J. Lu, Y. Xiong, S. Zhang, Y. Qian, X. Liu, J. Mater. Chem. **12**, 748 (2002). doi:10.1039/b105652m
30. C.J. Barrelet, Y. Wu, D.C. Bell, C.M. Lieber, J. Am. Chem. Soc. **125**, 11498 (2003). doi:10.1021/ja036990g
31. C. Ye, G. Meng, Y. Wang, Z. Jiang, L. Zhang, J. Phys. Chem. B **106**, 10338 (2002). doi:10.1021/jp0255785
32. Y. Wang, G. Meng, L. Zhang, C. Liang, J. Zhang, Chem. Mater. **14**, 1773 (2002). doi:10.1021/cm0115564
33. M.A. Malik, P. O'Brien, N. Revaprasadu, Chem. Mater. **14**, 2004 (2002). doi:10.1021/cm011154w
34. P. Reiss, J. Bleuse, A. Pron, Nano Lett. **2**, 781 (2002). doi:10.1021/nl025596y
35. M. Danek, K.F. Jensen, C.B. Murray, M.G. Bawendi, Chem. Mater. **8**, 173 (1996). doi:10.1021/cm9503137
36. A. Datta, S.K. Panda, S. Chaudhuri, J. Phys. Chem. C **111**, 17260 (2007). doi:10.1021/jp076093p
37. Y.J. Hsu, S.Y. Lu, Y.F. Lin, Adv. Funct. Mater. **15**, 1350 (2005). doi:10.1002/adfm.200400563
38. M.R. Kim, Y.M. Kang, D.J. Jang, J. Phys. Chem. C **111**, 18507 (2007). doi:10.1021/jp075218n
39. J. Zhan, X. Yang, D. Wang, S. Li, Y. Xie, Y. Xia, Y. Qian, Adv. Mater. **12**, 1348 (2000). doi:10.1002/1521-4095(200009)12:18<1348::AID-ADMA1348>3.0.CO;2-X
40. Y.J. Hsu, S.Y. Lu, Langmuir **20**, 194 (2004). doi:10.1021/la0347410
41. S. Kalele, S.W. Gosavi, J. Urban, S.K. Kulkarni, Curr. Sci. **91**, 1038 (2006). sici:0011-3891(20061025)91:8L.1038:NPSP;1-U
42. R.G. Xie, U. Kolb, J.X. Li, T. Basche, A. Mews, J. Am. Chem. Soc. **127**, 7480 (2005). doi:10.1021/ja042939g
43. R. Wang, J.H. Xin, Y. Yang, H. Liu, L. Xu, J. Hu, Appl. Surf. Sci. **227**, 312 (2004). doi:10.1016/j.apsusc.2003.12.012
44. H. Lachheb, E. Puzenat, A. Houas, M. Ksibi, E. Elaloui, C. Guillard, J.M. Hermman, Appl. Catal. B Environ. **31**, 145 (2001). doi:10.1016/S0926-3373(00)00276-9
45. C. Yogi, K. Kojima, N. Wada, H. Tokumoto, T. Takai, T. Mizoguchi, H. Tamiaki, Thin Solid Films **516**, 5881 (2008). doi:10.1016/j.tsf.2007.10.050
46. L.H. Kieth, W.A. Telliard, Environ. Sci. Technol. **13**, 416 (1979). doi:10.1021/es60152a601
47. X. Shen, L. Zhu, G. Liu, H. Yu, H. Tang, Environ. Sci. Technol. **42**, 1687 (2008). doi:10.1021/es071788p
48. Shen X, Zhu L, Li J, Tang H (2007) Chem. Commun. (Camb.) 1163. doi:10.1039/b615303h